ADVANCED FUNCTIONAL MATERIALS
www.afm-journal.de

Tunable Assembly of sp^3 Cross-Linked 3D Graphene Monoliths: A First-Principles Prediction

Xue Jiang, Jijun Zhao, Yan-Ling Li, and Rajeev Ahuja*

One of the biggest challenges in graphene applications is how one can fabricate 3D architectures comprising graphene sheets in which the resulting architectures have inherited graphene's excellent intrinsic properties but have overcome its shortcomings. Two series of 3D graphene monoliths (GMs) using zigzag or armchair graphene nanoribbons as building blocks and sp^3 carbon chains as junction nodes are constructued, and calculations based on first principles are performed in order to predict their mechanical and electronic properties. The perfect match between sp^2 nanoribbons and sp^3 linkers results in favorable energy and mechanical/dynamic stability. Owing to their tailored motifs, wine-rack-like pores, and rigid sp^3 linkers, these GMs possess high surface areas, appreciable mechanical strength, and tunable band gaps. Negative linear compressibilities in a wide range are found for the zigzag GMs. By solving the problems of zero gap and dimensionality of graphene sheets simultaneously, these GMs offer a viable strategy towards many applications, e.g., microelectronic devices, energy storage, molecular sieves, sensitive pressure detectors, and telecommunication line systems.

1. Introduction

Graphene, a 2D monolayer of carbon atoms with sp^2 hybridization, possesses outstanding mechanical, thermal, optical, and electrical properties, and it holds promise for a variety of applications, such as in microelectronic devices, energy storage, and chemical and biological sensors.[1,2] However, the broad range of application of graphene-based materials is hindered by two major drawbacks: 1) the zero band gap of pristine graphene;[3] and 2) the difficulty in integrating individual 2D graphene sheets into macroscopic structures.[4–6]

It has been demonstrated that an electronic gap in graphene can be opened by cutting a large graphene sheet into well-defined nanoribbons[7–9] or by transforming the hybridization state of carbon from sp^2 to sp^3 via chemical functionalization.[10–12] The electronic properties of a graphene nanoribbon sensitively rely on its width and edge structure.[7–9] Chemical functionalization of graphene, such as hydrogenation, fluorination, or oxidation, introduces sp^3 hybridized C−C bonds into the pristine sp^2 carbon network[10] and may tune the band gap from the middle-ultraviolet to near-infrared region.[11]

Self-assembly has been recognized as an effective strategy for the bottom–up synthesis of 3D macrostructures using graphene sheets as building blocks. So far, the 2D graphene sheets are usually assembled via physical linkers with van der Waals (vdW) forces.[13–16] The obtained 3D graphene assemblies exhibit large surface area, high porosity, and excellent electrochemical properties, but they lack some of the intrinsic merits of monolayer graphene sheets, such as high electrical conductivity and a superior Young's modulus. Recently, Worsley et al.[5,6] and Chen et al.[17] synthesized covalently bonded 3D networks of graphene, which posessed high electrical conductivity and a Young's modulus that are comparable to graphene, but the networks had a relatively lower surface area (~1000 m^2/g). Considering both the aforementioned physical/chemical stacking approaches and industrial needs, an ideal 3D graphene architecture should provide reasonable configuration modes, high specific surface areas, strong mechanical strength, and fast mass/electron transport kinetics.[4]

In this publication, we design two classes of 3D covalently interlinked graphene monoliths (GMs) by combining sp^2 zigzag and armchair graphene nanoribbons as building units and sp^3 carbon chains as junction nodes. These 3D all-carbon network materials, which have tunable pore size, controllable chirality and bonding type, favorable energetic/dynamical stability, and appreciable mechanical strength, provide an effective strategy for assembling 2D graphene sheets into 3D macrostructures. More importantly, these carbon allotropes are semiconductors with tunable band gaps, and some of them exhibit an unusual negative linear compressibility (NLC) under compression. All of these superior properties suggest promising applications in many fields, including microelectronic devices, energy storage,

Dr. X. Jiang, Prof. J. Zhao
Key Laboratory of Materials Modification by Laser, Ion and Electron Beams (Dalian University of Technology)
Ministry of Education
Dalian 116024, China
E-mail: jjzhao@dlut.edu.cn
Dr. X. Jiang, Prof. R. Ahuja
Department of Materials and Engineering
Royal Institute of Technology
Stockholm 10044, Sweden
Prof. Y.-L. Li
School of Physics and Electronic Engineering
Jiangsu Normal University
Xuzhou 221116, China
Prof. Y.-L. Li, Prof. R. Ahuja
Department of Physics and Astronomy
Box 516, Uppsala University
751 23, Uppsala, Sweden

DOI: 10.1002/adfm.201301077

molecular sieves, sensitive pressure detectors, and telecommunication line systems.

2. Results and Discussion

2.1. Structural Model and Stability

Inspired by the recently proposed carbon allotropes such as graphyne ($sp+sp^2$),[18] Y-carbon and TY carbon ($sp+sp^3$),[19] carbon foam (sp^2+sp^3),[20] C_{60} and nanotube polymers,[21,22] and open carbon frameworks,[4] we constructed two series of 3D porous allotropes of carbon. As shown in **Figure 1**, the motivation behind designing these bulk GMs was to integrate zigzag or armchair graphene nanoribbons as basic motifs with tetrahedrally coordinated sp^3 chains as cross linkers, producing ZGMs or AGMs, respectively. For each GM structure, a zigzag or armchair sp^3 chain is used as junction node, while its dangling bonds are terminated by the C−C bonds with the nanoribbon exhibiting the same chirality. With fixed junction nodes, one can easily tailor the width of the zigzag or armchair nanoribbons by inserting more six-membered rings (6MRs). Specifically, ZGMs containing 12, 20, and 28 atoms per unit cell (namely, ZGM-12, ZGM-20, and ZGM-28) correspond to a width of two, three, and four 6MRs, respectively; while AGMs with 12, 20, and 28 atoms per unit cell (namely, AGM-12, AGM-20, and AGM-28) contain 1.5, 2, and 2.5 6MRs, respectively. As a consequence, two series of infinite 1D channels (rhombus-shaped from top view) are formed along the <001> axis, and the 2D periodic arrangements of these 1D channels further constitute unique 3D wine-rack-like structures of GMs. In principle, many possible GMs of different pore sizes could be constructed. Here we considered ZGM-12, ZGM-20, ZGM-28, AGM-12, AGM-20, and AGM-28 as representative models for the sp^2/sp^3 hybrid 3D monolithic graphene (**Figure 2**). Intuitively, the adjustable structural parameters, such as chirality and width of nanoribbons, pore size, and arrangement of the 1D channels, would result in fascinating and tunable properties for these GM architectures, which we will demonstrate in the following discussions.

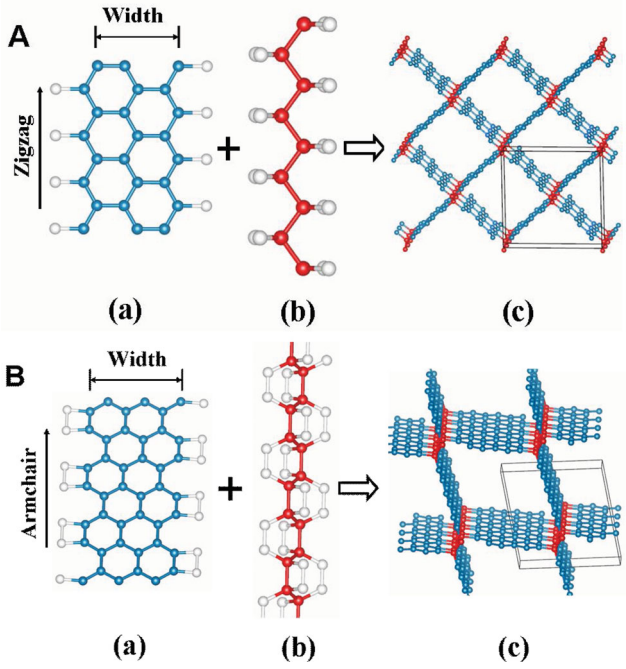

Figure 1. Schematic illustration of the formation of the GMs. A) ZGM-28 with zigzag graphene nanoribbons as building blocks. B) AGM-28 with armchair graphene nanoribbons as building blocks. a) Graphene nanoribbon building block with tunable width and direction; b) view of sp^3 linking chain; c) structure of ZGM-28 and of AGM-28. Blue and red represent carbon atoms corresponding to the nanoribbon building blocks and linker chains, respectively.

The structural parameters (space group, ratios of the number of sp^2 and sp^3 atoms to the total number of atoms within the unit cell, bond lengths, and mass density), cohesive energy, and electronic band gap of the six GM models obtained using calculations based on first principles are summarized in Table 2, where they are also compared with those of graphite and diamond. The detailed lattice parameters and coordinates are provided in **Table 1** as well. Taking ZGM-28 as an example (see **Figure 1**), the carbon atoms are located at the 4c (0.5, 0.54, 0.25), 8g (0.36, 0.65, 0.75), 8g (0.40, 0.39, 0.75), and 8g (0.27, 0.54. 0.25) sites. The 4c carbons form an sp^3 carbon chain, whereas the rest of carbon atoms belong to the zigzag graphene nanoribbons. The C−C bonds in the equilibrium structure of ZGM-28 have four different lengths: the shortest bonds are 1.42 and 1.45 Å within the nanoribbons; the intermediate ones are 1.51 Å connecting the sp^3 and sp^2 atoms; and the longest one is 1.52 Å along the sp^3 chain.

For a given number of atoms in a unit cell, the percentage of sp^3 atoms is the same for both series of the GM structures, i.e., 33% for ZGM-12 and AGM-12, 20% for ZGM-20 and AGM-20, and 14% for ZGM-28 and AGM-28. The zigzag and armchair GM assemblies differ in the detailed linking modes between sp^3 chains and sp^2 sheets. The connection between zigzag nanoribbons and sp^3 functional knot contains only 6MRs; however, there are some four-membered rings (4MRs) in the armchair GMs. The average bond angles of the sp^3 carbon atoms are 108.4°, 109.1°, 108.8°, 105.8°, 105.8°, and 107.2° for ZGM-12, ZGM-20, ZGM-28, AGM-12, AGM-20, and AGM-28, respectively. Obviously, the bond angles of AGMs deviate more from the ideal value of sp^3 hybridization (109.28°) than ZGMs.

Owing to the porous wine-rack-like configurations, the densities of ZGM-12, ZGM-20, ZGM-28, AGM-12, AGM-20, and AGM-28 are 2.59, 1.93, 1.53, 2.23, 1.70, and 1.36 g/cm^3, respectively, which are comparable to those of graphite (2.20 g/cm^3), fullerene solid (1.65 g/cm^3), and nanotube bundles (1.33 g/cm^3).[23] Accordingly, the specific areas of these GMs (≈997–2171 m^2/g) are generally larger than previously reported covalent 3D graphene assemblies (584,[15] 850,[17] 964,[24] 1199,[6] and 1300 m^2/g).[5] As nanoribbon width (and pore size) further increases, the surface area of these GMs gradually approach the graphene value of 2630 m^2/g.[25] Hence, these GM allotropes with low densities and high surface areas are expected to have promising applications in areas of energy storage/conversion, shaped-selective catalysts, molecular sieves, and absorbents.

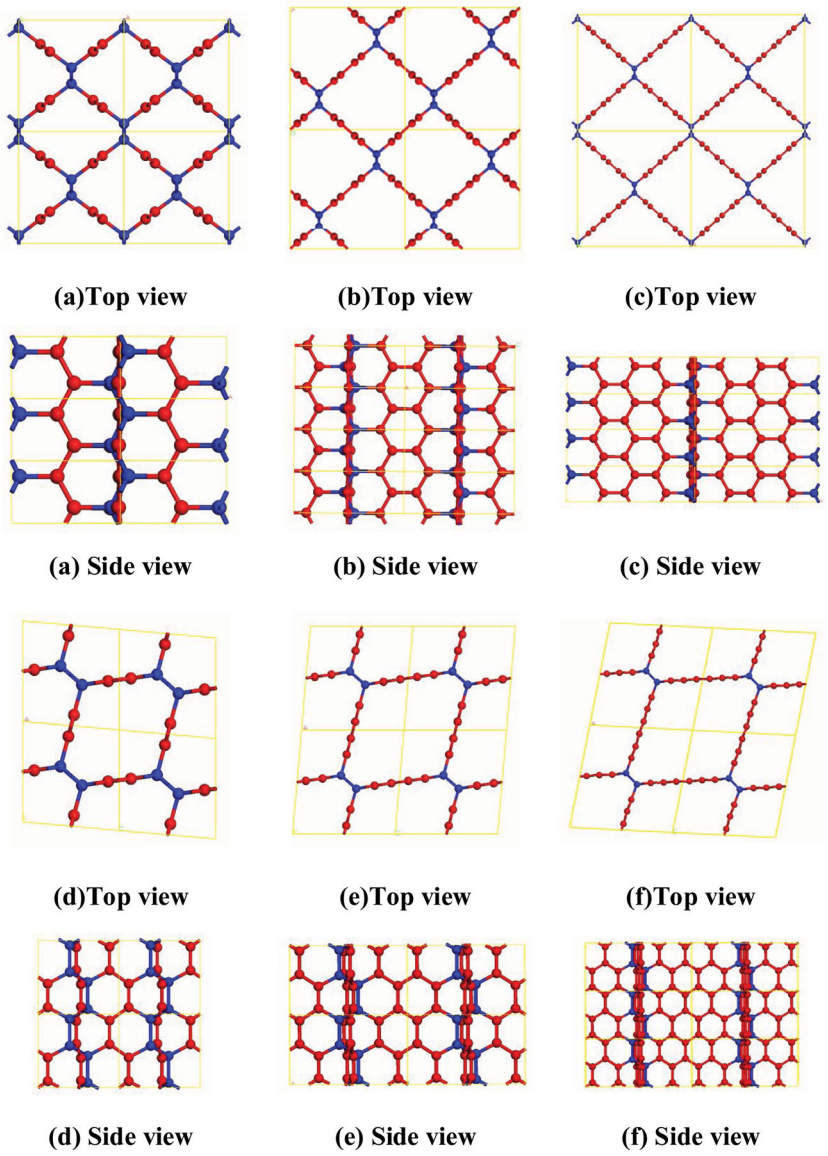

Figure 2. Structural models of GMs with different widths of zigzag and armchair graphene: a) ZGM-12, b) ZGM-20, c) ZGM-28, d) AGM-12, e) AGM-20, and f) AGM-28. Blue and red represent carbon atoms corresponding to linker chains and the nanoribbon building blocks, respectively.

Figure 3 displays the equations of states for all six GMs, graphite, and diamond. Along with the cohesive energies summarized in **Table 2**, one can see that these 3D graphene assemblies are slightly less stable than diamond and graphite by only ≈0.1–0.3 eV/atom. With the same sp^3/sp^2 ratio, the GMs constructed from zigzag nanoribbons are more stable than the armchair ones by ≈0.06–0.19 eV/atom. This is due to the incorporation of energetically unfavorable 4MRs and the larger deviation of sp^3 bond angles in the AGMs. As the width of nanoribbon increases, the thermodynamic stability of both ZGMs and AGMs further increases and gradually approaches the limit of infinite graphene. Also note that these new GM phases possess larger cohesive energies than the recently proposed low-density carbon allotropes, such as T-carbon,[26] Bct-C4,[27] H6,[28] K4-carbon,[28] sp^2-diamond,[29] Y-carbon,[19] TY-carbon,[19] and the 3D C_{60} polymer.[21,22] Detailed comparisons can be found in the Supporting Information (Table S1).

We further assess the dynamic and mechanical stability of these GMs by computing their phonon dispersion and elastic constants (see Figure S1 and Table S2 in the Supporting Information). As shown in the Supporting Information, there is no negative frequency throughout the entire Brillioun zone, and all the independent elastic constants satisfy the well-known Born stability criteria,[30] confirming that all GMs explored are dynamically and mechanically stable at ambient conditions.

The satisfactory stability of these graphene assemblies implies that they are feasible from the theoretical point of view. It is interesting to point out that the experimentally synthesized 3D C_{60} polymer[22] with a sp^3/sp^2 ratio close to that of AGM-28 or ZGM-28 is even less stable than its GM counterparts by ≈0.2–0.26 eV/atom (see Table S1 in the

Table 1. Space group, lattice constants, and Wyckoff positions of ZGM-12, ZGM-20, ZGM-28, AGM-12, AGM-20, and AGM-28.

Systems	Space group	Lattice constants [Å; °]	Wyckoff position
ZGM-12	*Cmcm*	5.9410, 6.3050, 2.4669	4c (0, 0.0717, 0.7500); 8g (0.2051, 0.7838, 0.2500)
ZGM-20	*Imma*	2.4658, 9.2871, 9.0209	4e (0, 0.4394, 0.0511); 8h (0, 0.3813, 0.3998); 8h (0.5000, 0.2500, 0.2017)
ZGM-28	*Cmcm*	12.2209, 12.1338, 2.4647	8g (0.3605, 0.6528, 0.7500); 8g (0.4035, 0.3851, 0.7500); 8g (0.2717, 0.2691. 0.2500); 4c (0.5000, 0.5369, 0.2500)
AGM-12	$P2_1/m$	4.9239, 4.4458,4.9215; 94.87°	4f (0.8908, 0.9030, 0.4716); 4f (0.5235, 0.4104, 0.1181); 4f (0.5846, 0.9322, 0.3888)
AGM-20	$P2_1/m$	7.3814, 4.3404, 7.3600; 85.03°	4f (0.7641, 0.9076, 0.4586); 4f (0.5344, 0.4101, 0.2430); 4f (0.5638, 0.9328, 0.4203); 4f (0.4885, 0.4168, 0.9183); 4f (0.0805, 0.9140, 0.5140)
AGM-28	$P2_1/m$	9.8339, 4.3236, 9.7982; 81.56°	4f (0.5065, 0.4160, 0.0620); 4f (0.7004, 0.9088, 0.4625); 4f (0.5322, 0.4113, 0.3054); 4f (0.5501, 0.9329, 0.4387); 4f (0.4807, 0.4179, 0.8152); 4f (0.1828, 0.9150, 0.5228); 4f (0.9386, 0.9161, 0.4923)

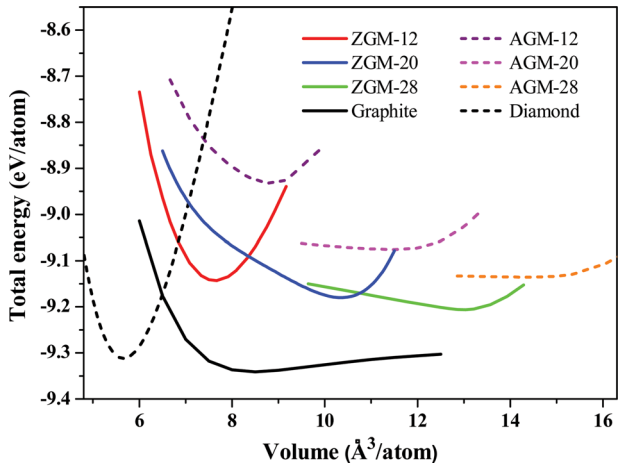

Figure 3. The equations of states of graphite, ZGM-12, ZGM-20, ZGM-28, AGM-12, AGM-20, and AGM-28.

SI). Although the synthesis of such 3D graphene monoliths with tunable pore size and nanoribbon chirality is a big challenge for experimentalists, there is still some evidence to support our hypothetical sp^2/sp^3 mixed structures.[17,22,31–35] Chen et al.[17] reported the formation of 3D macroscopic graphene structures using a template-directed chemical vapor deposition (CVD) approach. Nickel foam was used as the favorable scaffold to deposit wrinkled graphene film, and after etching the underlying nickel, such a porous graphene monolith was produced.[17,31] In the experiment by Xiao et al., the predefined 3D graphitic monolith formed by 3D amorphous carbon structures was conformally sputtered with nickel. Afterwards, acidic etching can chemically convert those graphitic monolith precursors into well-defined hollow interconnected 3D multilayered graphene products with pore sizes at the nanometer scale.[35]

Also note that the geometry and pore size/shape of the present GMs rather resemble some recently synthesized metal organic frameworks (MOFs) or porous coordination polymers.[32,33,34] The major difference is that our GMs are all-carbon materials, while those MOFs contain metal ions and organic units. Thus, it might be possible to first synthesize a 2D MOF of geometry similar to our GM using hydrothermal or solvothermal techniques and then replace the metal ions and other non-carbon elements using a carefully controlled substitutional reaction in order to achieve all-carbon GM materials. In particular, the postsynthetic ligand- and metal-ion-exchange processes in MOFs, in which secondary-building-unit metals are replaced, seems to be a promising approach along this line.[33] Even so, it is still hard to experimentally achieve the perfect wine-rack-like configurations of our theoretical predictions because different patterning techniques of graphene ribbons and inevitable defects on edge sites or junction regions would induce some imperfection in the 3D graphene networks and would result in a lower mass density of the real graphene monolith materials, which would further affect their electronic and mechanical properties.

2.2. Electronic Properties

For future applications in microelectronics, it is crucial to explore the electronic band structures of these 3D graphene assemblies. HSE06 calculations (Heyd–Scuseria–Ernzerhof) show that they are semiconductors with direct gaps, i.e., 0.49, 1.06, 0.99, 1.66, 2.78, and 2.78 eV for ZGM-12, ZGM-20, ZGM-28, AGM-12, AGM-20, and AGM-28, respectively. The difference between these two kinds of GMs indicates that they inherit the chirality dependence of electronic properties of graphene nanoribbons.[7–9] However, the amplitude of the band gap is affected by many competing factors simultaneously. One of them is of course the quantum confinement effect, i.e., the energy gap of the nanoribbon decreases as width increases.[7–9] Another important reason for gap variation is the ratio of sp^2 to sp^3 carbon atoms; that is, inserting more sp^2 carbon atoms between sp^3 junctions reduces the band gap. This can be easily understood by the fact that the sp^3 phase of carbon (diamond as insulator) and the sp^2 phase of carbon (graphene as semimetal) possess a large gap of 5.69 eV (HSE06 value) and a zero gap, respectively. Moreover, the C−C bond lengths in the equilibrium configurations of these 3D GMs deviate from the conventional values for sp^2 graphene (1.42 Å) and sp^3 diamond

Table 2. Space group, mass density, ratios (R) of sp^2 and sp^3 atoms relative to the number of C atoms in the unit cell, C−C bond lengths, cohesive energy per carbon (E_c), and band gap (E_g) of the 3D zigzag and armchair GMs, diamond, and graphite. In the last column, the values inside and outside the parentheses are the energy band gaps from HSE06 (with Heyd–Scuseria–Ernzerhof hybrid functionals) and PBE (Perdew–Burke–Ernzerhof functionals) calculations, respectively.

Systems	Space group	Density [g/cm^3]	R_{sp3} [%]	R_{sp2} [%]	Bond lengths [Å]	E_c [eV/atom]	E_g [eV]
ZGM-12	*Cmcm*	2.59	33	67	1.41; 1.52; 1.53	8.99	0.36 (0.49)
ZGM-20	*Imma*	1.93	20	80	1.42; 1.45; 1.51; 1.52	9.07	0.8 (1.06)
ZGM-28	*Cmcm*	1.53	14	86	1.42; 1.44; 1.51; 1.52	9.11	0.70 (0.99)
AGM-12	$P2_1/m$	2.23	33	67	1.36–1.62	8.80	0.39 (1.66)
AGM-20	$P2_1/m$	1.70	20	80	1.39–1.59	8.98	1.13 (2.78)
AGM-28	$P2_1/m$	1.36	14	86	1.37–1.58	9.05	1.59 (2.78)
Graphite	$P6_3/mmc$	2.24	0	100	1.42	9.23	0 (0)
Diamond	$Fd\bar{3}m$	3.52	100	0	1.55	9.20	4.59 (5.69)

(1.55 Å). As listed in Table 1, the sp^2 C−C bond lengths are ≈1.36–1.51 Å, and the sp^3 C−C bond lengths range between 1.52 and 1.62 Å. Such asymmetrical strain and shear deformation on the structural units of carbon atoms might open the band gap.[36,37] The partial density of states (PDOS) of ZGM-28 shown in the **Figure 4** further illustrates that almost all conducting states in the vicinity of the Fermi level originate from the $2p_x$ and $2p_z$ orbitals of the carbon atoms bonded to the sp^3 chains, where the largest deviations from the standard sp^2 C−C bond length occur. In short, the band gap of GMs can be tailored by the nanoribbon width, sp^3/sp^2 ratio, and detailed atomic configurations; which may cancel each other to some extent. The flexible band gaps of these 3D graphene assemblies imply new opportunities in band engineering for microelectronic and photonic devices.

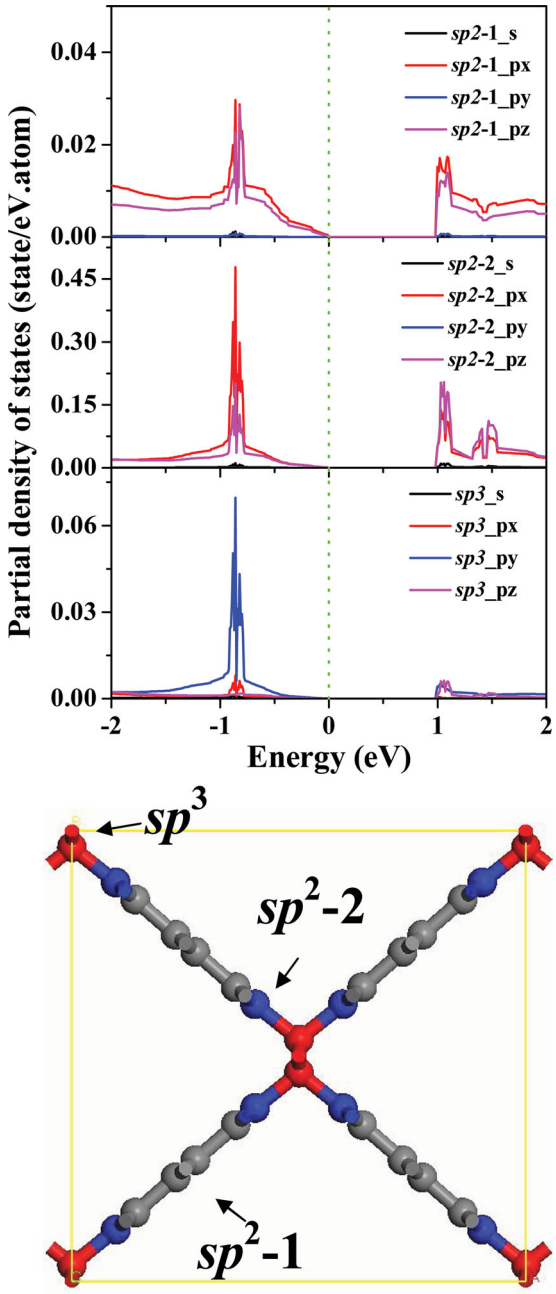

Figure 4. Partial density of states (PDOS) of ZGM-28 for three different types of carbon atoms from HSE06 calculations. The green vertical dotted line indicates the Fermi level. sp2-1, sp2-2, sp3 represent the sp^2 carbon atoms in the center sites of the graphene nanoribbons (grey atoms in the lower structural model), the sp^2 carbon atoms at the edge sites of the graphene nanoribbons (blue atoms), and the sp^3 carbon atoms (red atoms), respectively.

2.3. Mechanical Behavior

Graphene is known to possess exceptional mechanical properties with an ultrahigh in-plane Young's modulus of ≈1.0 TPa.[38,39] As a 3D stacked assembly of graphene held together by vdW interactions, graphite has a large Young's modulus within the basal plane but a very low shear elastic modulus (C_{44} = 3 GPa from our calculations, as shown in Table S2 (SI) and C_{44} = 5 GPa from experiment)[40] between the graphene layers, which makes graphite an ultrasoft material. In contrast, diamond with sp^3 hybridization is the hardest material in nature. Hence, it would be interesting to explore the mechanical behavior of these sp^2/sp^3 mixed GMs and to investigate the effect of the sp^2/sp^3 ratio. The theoretical Young's moduli and ideal strengths of six GMs are listed in **Table 3**. Excitingly, the calculated Young's modulus (1172 GPa) and ideal strength (133.38 GPa) for ZGM-12 along the <001> orientation are comparable to the values of graphene (1164 and 117.26 GPa) and diamond (1115 and 230 GPa) along their strongest orientations. As the pore size increases (i.e., mass density and the percentage of sp^3 carbon atoms decreases), the Young's modulus and ideal strength of the 3D graphene monoliths are weakened (see Table 3). For instance, the Young's modulus of ZGMs along the <001> direction reduces from 1172 GPa for ZGM-12 to 688 GPa for ZGM-28, while the corresponding ideal strength drops from 133.38 to 76.9 GPa.

It is noticeable that these porous graphene monoliths are much harder than graphite by about two orders of magnitude, as demonstrated by the calculated shear modulus of ≈77–268 GPa for GMs and 4 GPa for graphite. In other words, the 3D graphene assemblies designed here not only retain the superior mechanical performance within the basal plane, but also gain great reinforcement in their axial directions via sp^3 covalently bonded linkers. Such a significant enhancement of the shear modulus (and consequently hardness)[41] of the 3D connected phases of graphene with regard to graphite is surely beneficial for future material applications.

Interestingly, the Young's modulus and ideal strength normal to the three principal directions for those GM structures are highly anisotropic and chirality-dependent. Both the Young's modulus and ideal strength show highest values along the <001> direction (i.e., the 1D channel axis), which are about twice of those along the other two crystallographic axes, i.e., <100> and <010>. For example, the ideal tensile strengths are σ<100> = 35.04 GPa, σ<010> = 38.43 GPa, σ<001> = 76.9 GPa for ZGM-28 and σ<100> = 24.17 GPa, σ<010> = 25.39 GPa, σ<001> = 50.76 GPa for AGM-28. Obviously, the observed elastic anisotropy of these 3D porous GMs originates from their

Table 3. Young's modulus [GPa], ideal fracture strength [GPa], critical fracture strain and linear compressibility [TPa^{-1}] of our representative 3D GMs along the crystallographic directions <100>, <010>, and <001>.

System	Fracture strength (Strain)			Young's modulus			Linear compressibility		
	<100>	<010>	<001>	<100>	<010>	<001>	$\beta_{<100>}$	$\beta_{<010>}$	$\beta_{<001>}$
ZGM-12	69.86 (35%)	72.15 (27%)	133.38 (25%)	349	480	1172	0.5	2.2	0.7
ZGM-20	47.66 (35%)	49.76 (30%)	99.8 (25%)	225	280	872	–18.4	12.3	1
ZGM-28	35.04 (35%)	38.43 (27%)	76.9 (25%)	165	218	688	–37.6	56.7	1.2
AGM-12	48.32 (22%)	55.94 (20%)	69.42 (17%)	340	468	677	3.4	4.7	1.1
AGM-20	33.92 (17%)	35.94 (15%)	59.84 (17%)	258	312	640	24.5	17.1	2.3
AGM-28	24.17 (12%)	25.39 (15%)	50.76 (17%)	248	212	536	75.4	50.5	3.9

structural anisotropy. Also note that the anisotropy of ZGMs is slightly stronger than AGMs.

2.4. Novel Negative Linear Compressibility

We further explore the mechanical behavior of these GMs by applying hydrostatic pressure up to 8 GPa. As two representatives, the lattice parameters for ZGM-28 and AGM-20 as functions of cell volume are displayed in **Figure 5**. Upon compression, the lattice parameters of these GMs exhibit pronounced anisotropic variations and even expand along the <100> direction for selected GMs. The values of linear compressibility ($\beta = -dL/LdP$, where L is a lattice parameter and P is pressure) along three principal directions are summarized in Table 3. Unlike the armchair series and ZGM-12 with all positive β values along three axes, unusual NLC values of –37.6 and –18.4 TPa^{-1} along the <100> orientation were obtained for ZGM-28 and ZGM-20, respectively.

Due to their unique wine-rack-like configurations, the linker length of these 3D graphene monoliths remain nearly constant under hydrostatic compression while the pore channels deform substantially to undertake the external loading (see Figure 5), as proposed by Baughman et al.[42] For example, the sp^3 carbon chain along the <001> axis of ZGM-28 is rather rigid with a very small linear compressibility of 1.2 TPa^{-1}, which is in the typical order of magnitude for inorganic solids.[43] Then, the overall narrowing of the "wine-rack" pore results in a contraction in the <010> direction with a positive linear compressibility (β = 56.7 TPa^{-1}) and simultaneously an expansion in the <100> direction with β = –37.6 TPa^{-1} to keep the length of rigid sp^3 linker invariant. This effect is clearly demonstrated by the dihedral angle of the "wine-rack" channel, which changes from 101.89° to 107.52° for ZGM-28 as the volume reduces from

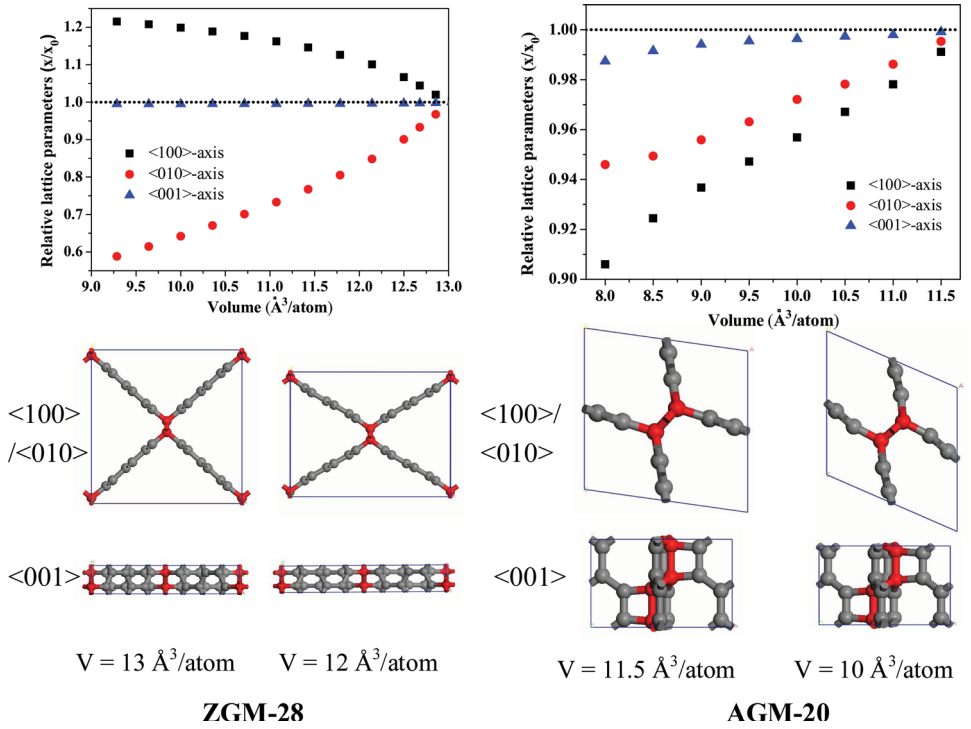

Figure 5. Top: Individual lattice parameters (x/x_0) as functions of volume (V). Bottom: Detailed changes of the atomic structures under compression for ZGM-28 and AGM-20.

13.21 to 12.14 Å^3/atom. Similar compression-induced deformation of dihedral angles is also observed in the armchair GMs, e.g., from 116.17° at a volume of 11.5 Å^3/atom to 126.39° at 10 Å^3/atom for AGM-20. However, positive linear compressibility along the <100> axis is obtained for the AGM series. This can be attributed to the specific symmetry of the wine-rack-like framework. As monoclinic crystals, hydrostatic compression of the AGM framework triggers not only breathing of the "wine-rack" pores but also shearing of the unit cell (i.e., the cell angle changes from 81.8° at a volume of 11.5 Å^3/atom to 66.45° at 10 Å^3/atom for AGM-20). The latter effect would compensate deformation of the wine-rack-like framework and recover the conventional positive linear compressibility.

Moreover, linear compressibility of these 3D graphene monoliths sensitively relies on its pore size (or nanoribbon width). Along the <010> and <001> directions, β increases with increasing pore size, whereas it drops drastically from 0.5 TPa^{-1} for ZGM-12 to −18.4 TPa^{-1} for ZGM-20 and −37.6 TPa^{-1} for ZGM-28 along the unusual <100> orientation. As the pore size further increases, our first-principles calculations revealed that the NLC value would keep reducing to −51.0 TPa^{-1} for ZGM-36 and −66.1 TPa^{-1} for ZGM-44. For comparison, the previously reported NLC values are −1.2 TPa^{-1} for elemental Se,[44] −1.8 TPa^{-1} for $[NH_4][Zn(HCOO)_3]$,[45] −12 TPa^{-1} for $KMn[Ag(CN)_2]_3$,[46] −42 TPa^{-1} for $Zn[Au(CN)_2]_2$,[47] −75 TPa^{-1} for $Ag_3[Co(CN)_6]$,[48] and −257 TPa^{-1} for the MIL-53 framework.[49] Certainly, the tunable linear compressibility for ZGMs in a wide range can satisfy parameter requirements for a variety of applications, such as extremely sensitive pressure detectors, telecommunication line systems, and optical materials with very high refractive index.[44–49]

3. Conclusion

To summarize, two series of 3D graphene monoliths were constructed by self-assembling zigzag or armchair graphene nanoribbons. The resulting assemblies go beyond the widely used physical integration involving vdW forces, and are held together using sp^3 carbon junctions instead. Such assemblies of graphene layers may fulfill the dream of producing 3D graphene materials with high porosity, high specific surface area, moderate mechanical strength, and suitable band gap, having inherited the intrinsic merits of graphene and having overcome its shortcomings. The optimal combinations of sp^2 graphene nanoribbons and sp^3 linkers would result in many promising applications in microelectronic and photonic devices, energy storage, and molecular sieves. Moreover, ZGMs are identified as flexible materials with negative linear compressibility due to their unique wine-rack-like structures and anisotropic mechanical strength. The tunable NLC of zigzag graphene monoliths is also anticipated to have applications in sensitive pressure detectors, telecommunication line systems, and optical materials.

4. Computational Method

The equilibrium structures of two kinds of graphene monoliths were optimized using density functional theory (DFT) implemented in the VASP (Vienna ab initio simulation package) code.[50] The exchange-correlation interaction was treated by the Perdew–Burke–Ernzerhof (PBE) functional.[51] We employed the projected augmented wave (PAW) method[52] with an energy cutoff of 700 eV to describe the electron wave function. In all calculations, self-consistency was achieved with a tolerance for the total energy of at least 0.001 meV and the Hellmann–Feyman forces less than 0.001 eV/Å. Since conventional DFT methods usually underestimate the band gap of a semiconductor,[53] we further computed the band gap using the HSE06 hybrid functional.[54] The **k** point grids of $8 \times 8 \times 10$, $6 \times 6 \times 10$, $4 \times 4 \times 10$, $8 \times 8 \times 8$, $6 \times 6 \times 8$, and $4 \times 4 \times 8$ were used for the ZGM-12, ZGM-20, ZGM-28, AGM-12, AGM-20, and AGM-28, respectively. For each equilibrium crystal structure, phonon dispersion curves were computed using the direct supercell method as implemented in the Phonopy program.[55]

Supporting Information

Supporting Information is available from the Wiley Online Library or from the author.

Acknowledgements

The authors thank the Swedish National Infrastructure for Computing (SNIC), the Program for Changjiang Scholars and Innovative Research Team in University of China, the National Natural Science Foundation of China (No. 11134005 and 11047013), the Fundamental Research Funds for the Central Universities of China (No. DUT12YQ05), the Swedish Research Council (VR), and the Priority Academic Program Development of Jiangsu Higher Education Institutions (PAPD).

Received: March 28, 2013
Revised: May 11, 2013
Published online: June 20, 2013

[1] D. Chen, L. Tang, J. Li, *Chem. Soc. Rev.* **2010**, *39*, 3157.
[2] Y. Sun, Q. Wu, G. Shi, *Energ. Environ. Sci.* **2011**, *4*, 1113.
[3] K. S. Novoselov, A. K. Geim, S. V. Morozov, D. Jiang, M. I. Katsnelson, I. V. Grigorieva, S. V. Dubonos, A. A. Firsov, *Nature* **2005**, *438*, 197.
[4] B. Kuchta, L. Firlej, A. Mohammadhosseini, P. Boulet, M. Beckner, J. Romanos, P. Pfeifer, *J. Am. Chem. Soc.* **2012**, *134*, 15130.
[5] M. A. Worsley, S. O. Kucheyev, H. E. Mason, M. D. Merrill, B. P. Mayer, J. Lewicki, C. A. Valdez, M. E. Suss, M. Stadermann, P. J. Pauzauskie, J. H. Satcher, J. Biener, T. F. Baumann, *Chem. Commun.* **2012**, *48*, 8428.
[6] M. A. Worsley, T. Y. Olson, J. R. I. Lee, T. M. Willey, M. H. Nielsen, S. K. Roberts, P. J. Pauzauskie, J. Biener, J. H. Satcher, T. F. Baumann, *J. Phys. Chem. Lett.* **2011**, *2*, 921.
[7] Y. W. Son, M. L. Cohen, S. G. Louie, *Phys. Rev. Lett.* **2006**, *97*, 216803.
[8] L. Yang, C. H. Park, Y. W. Son, M. L. Cohen, S. G. Louie, *Phys. Rev. Lett.* **2007**, *99*, 186801.
[9] A. H. Castro Neto, F. Guinea, N. M. R. Peres, K. S. Novoselov, A. K. Geim, *Rev. Mod. Phys.* **2009**, *81*, 109.
[10] R. Balog, B. Jorgensen, L. Nilsson, M. Andersen, E. Rienks, M. Bianchi, M. Fanetti, E. Laegsgaard, A. Baraldi, S. Lizzit, Z. Sljivancanin, F. Besenbacher, B. Hammer, T. G. Pedersen, P. Hofmann, L. Hornekaer, *Nat. Mater.* **2010**, *9*, 315.

[11] H. Gao, L. Wang, J. Zhao, F. Ding, J. Lu, *J. Phys. Chem. C* **2011**, *115*, 3236.
[12] Y. Wang, M. Jaiswal, M. Lin, S. Saha, B. Özyilmaz, K. P. Loh, *ACS Nano* **2012**, *6*, 1018.
[13] Z. Tang, S. Shen, J. Zhuang, X. Wang, *Angew. Chem.* **2010**, *122*, 4707.
[14] J. L. Vickery, A. J. Patil, S. Mann, *Adv. Mater.* **2009**, *21*, 2180.
[15] M. A. Worsley, P. J. Pauzauskie, T. Y. Olson, J. Biener, J. H. Satcher, T. F. Baumann, *J. Am. Chem. Soc.* **2010**, *132*, 14067.
[16] F. Liu, T. S. Seo, *Adv. Funct. Mater.* **2010**, *20*, 1930.
[17] Z. Chen, W. Ren, L. Gao, B. Liu, S. Pei, H. M. Cheng, *Nat. Mater.* **2011**, *10*, 424.
[18] F. Diederich, M. Kivala, *Adv. Mater.* **2010**, *22*, 803.
[19] J. Y. Jo, B. G. Kim, *Phys. Rev. B* **2012**, *86*, 075151.
[20] Z. Zhu, D. Tománek, *Phys. Rev. Lett.* **2012**, *109*, 135501.
[21] Z. Zhao, B. Xu, L. M. Wang, X. F. Zhou, J. He, Z. Liu, H. T. Wang, Y. Tian, *ACS Nano* **2011**, *5*, 7226.
[22] S. Yamanaka, A. Kubo, K. Inumaru, K. Komaguchi, N. S. Kini, T. Inoue, T. Irifune, *Phys. Rev. Lett.* **2006**, *96*, 076602.
[23] S. H. Lee, D. H. Lee, W. J. Lee, S. O. Kim, *Adv. Funct. Mater.* **2011**, *21*, 1338.
[24] L. Zhang, G. Shi, *J. Phys. Chem. C* **2011**, *115*, 17206.
[25] X. Cao, Y. Shi, W. Shi, G. Lu, X. Huang, Q. Yan, Q. Zhang, H. Zhang, *Small* **2011**, *7*, 3163.
[26] X.-L. Sheng, Q. B. Yan, F. Ye, Q. R. Zheng, G. Su, *Phys. Rev. Lett.* **2011**, *106*, 155703.
[27] R. Hoffmann, T. Hughbanks, M. Kertesz, P. H. Bird, *J. Am. Chem. Soc.* **1983**, *105*, 4831.
[28] B. Winkler, C. J. Pickard, V. Milman, G. Thimm, *Chem. Phys. Lett.* **2001**, *337*, 36.
[29] C. He, L. Sun, C. Zhang, J. Zhong, *Phys. Chem. Chem. Phys.* **2013**, *15*, 680.
[30] Z. Wu, E. Zhao, H. Xiang, X. Hao, X. Liu, J. Meng, *Phys. Rev. B* **2007**, *76*, 054115.
[31] M. T. Pettes, H. Ji, R. S. Ruoff, L. Shi, *Nano Lett.* **2012**, *12*, 2959.
[32] E. D. Bloch, D. Britt, C. Lee, C. J. Doonan, F. J. Uribe-Romo, H. Furukawa, J. R. Long, O. M. Yaghi, *J. Am. Chem. Soc.* **2010**, *132*, 14382.
[33] M. Kim, J. F. Cahill, H. Fei, K. A. Prather, S. M. Cohen, *J. Am. Chem. Soc.* **2012**, *134*, 18082.
[34] A. Shigematsu, T. Yamada, H. Kitagawa, *J. Am. Chem. Soc.* **2012**, *134*, 13145.
[35] X. Xiao, T. E. Beechem, M. T. Brumbach, T. N. Lambert, D. J. Davis, J. R. Michael, C. M. Washburn, J. Wang, S. M. Brozik, D. R. Wheeler, D. B. Burckel, R. Polsky, *ACS Nano* **2012**, *6*, 3573.
[36] G. Gui, J. Li, J. Zhong, *Phys. Rev. B* **2008**, *78*, 075435.
[37] G. Cocco, E. Cadelano, L. Colombo, *Phys. Rev. B* **2010**, *81*, 241412.
[38] F. Liu, P. Ming, J. Li, *Phys. Rev. B* **2007**, *76*, 064120.
[39] C. Lee, X. Wei, J. W. Kysar, J. Hone, *Science* **2008**, *321*, 385.
[40] A. Bosak, M. Krisch, M. Mohr, J. Maultzsch, C. Thomsen, *Phys. Rev. B* **2007**, *75*, 153408.
[41] X. Jiang, J. Zhao, X. Jiang, *Comp. Mater. Sci.* **2011**, *50*, 2287.
[42] R. H. Baughman, S. Stafström, C. Cui, S. O. Dantas, *Science* **1998**, *279*, 1522.
[43] R. E. Newnham, *Properties of Materials*, Oxford University Press, Oxford **2005**.
[44] D. R. McCann, L. Cartz, R. E. Schmunk, Y. D. Harker, *J. Appl. Phys.* **1972**, *43*, 1432.
[45] W. Li, M. R. Probert, M. Kosa, T. D. Bennett, A. Thirumurugan, R. P. Burwood, M. Parinello, J. A. K. Howard, A. K. Cheetham, *J. Am. Chem. Soc.* **2012**, *134*, 11940.
[46] A. B. Cairns, A. L. Thompson, M. G. Tucker, J. Haines, A. L. Goodwin, *J. Am. Chem. Soc.* **2011**, *134*, 4454.
[47] A. B. Cairns, J. Catafesta, C. Levelut, J. Rouquette, A. van der Lee, L. Peters, A. L. Thompson, V. Dmitriev, J. Haines, A. L. Goodwin, *Nat. Mater.* **2013**, *12*, 212.
[48] A. L. Goodwin, D. A. Keen, M. G. Tucker, *Proc. Natl. Acad. Sci. USA* **2008**, *105*, 18708.
[49] A. U. Ortiz, A. Boutin, A. H. Fuchs, F. X. Coudert, *Phys. Rev. Lett.* **2012**, *109*, 195502.
[50] G. Kresse, D. Joubert, *Phys. Rev. B* **1999**, *59*, 1758.
[51] J. P. Perdew, J. A. Chevary, S. H. Vosko, K. A. Jackson, M. R. Pederson, D. J. Singh, C. Fiolhais, *Phys. Rev. B* **1992**, *46*, 6671.
[52] P. E. Blöchl, *Phys. Rev. B* **1994**, *50*, 17953.
[53] R. W. Godby, M. Schlüter, L. J. Sham, *Phys. Rev. Lett.* **1986**, *56*, 2415.
[54] J. Paier, M. Marsman, K. Hummer, G. Kresse, I. C. Gerber, J. G. Angyan, *J. Chem. Phys.* **2006**, *124*, 154709.
[55] A. Togo, F. Oba, I. Tanaka, *Phys. Rev. B* **2008**, *78*, 134106.